Applied Catalysis B: Environmental 152–153 (2014) 271–279

Contents lists available at ScienceDirect

Applied Catalysis B: Environmental

journal homepage: www.elsevier.com/locate/apcatb

Highly efficient light-induced hydrogen evolution from a stable Pt/CdS NPs-co-loaded hierarchically porous zeolite beta

Xiaoxia Zhou, Hangrong Chen*, Yuanyuan Sun, Kun Zhang, Xiangqian Fan, Yan Zhu, Yu Chen, Guiju Tao, Jianlin Shi

State Key Laboratory of High performance Ceramics and Superfine Microstructures, Shanghai Institute of Ceramics, Chinese Academy of Sciences, Shanghai 200050, PR China

ARTICLE INFO

Article history:
Received 15 October 2013
Received in revised form 6 January 2014
Accepted 13 January 2014
Available online 22 January 2014

Keywords:
H_2 evolution
Mesoporous beta
CdS
Pt
Water splitting

ABSTRACT

The CdS and Pt NPs have been homogeneously anchored and highly dispersed into the mesopore channels of hierarchically porous zeolite Beta by a facile successional two-step pore modification technology. A highly efficient and stable H_2 evolution of 3.09 mmol/h/$g_{catalyst}$ has been successfully achieved by using the prepared novel catalyst under sunlight irradiation. It is believed that the highly dispersive CdS and Pt NPs and the synergetic catalytic effect between them, as well as the interaction between CdS species and zeolite matrix, contribute to the enhanced separation and transfer of photoelectrons and holes, and therefore improving its electrochemical properties and H_2 evolution rate. Besides, and this novel hierarchical pore structure of zeolite Beta serving as a host can effectively protect CdS NPs from photocorrosion, thus exhibiting high stability in the catalytic system.

1. Introduction

Photocatalytic water-splitting for the clean, low-cost, and environment-friendly production of hydrogen offers promising solutions to the solar energy conversion and storage as well as to the hydrogen supply as a fuel for proton exchange membrane fuel cells. Overall, water splitting using semiconductor-based photocatalysts is one of the most popular routes for hydrogen evolution using solar energy [1]. However, most of the reported semiconductor photocatalysts, such as Ba-doped $Sr_2Nb_2O_7$ [2], $NiO/NaTaO_3$ [3], *etc.*, show a rather low photocatalytic activity for water splitting under sunlight irradiation. The key issues related to the problem are the low efficiency in the solar energy utilization and the limited charge separation efficiency upon photo-excitation, which is determined by the intrinsic electronic and structural properties of semiconductors [1e]. Therefore, it remains a major challenge to develop an excellent photocatalyst that can sufficiently harvest sunlight and effectively promote charge separation.

To effectively utilize solar energy, it is essential to develop a photocatalyst of appropriate band gap for the efficient sunlight absorption under the applied photocatalytic reaction conditions. Semiconductor CdS, as an attractive photocatalyst material, has been explored extensively in photocatalytic water splitting, since it has a relatively narrow band gap (2.4 eV) and a suitable conduction band potential to reduce H_2O [4]. However, there are several critical issues that limit the H_2 evolution rate enhancement on pure CdS particles. For example, the easy aggregation among CdS particles lead to reduced surface areas and increased recombination rates of photocharges. Beyond that, there is an inherent drawback for CdS-based photocatalysts, *i.e.*, the photocorrosion problem [5]. The sulfide ion can be easily oxidized by photogenerated holes which make CdS very unstable as a photocatalyst and consequently greatly limit its practical application. Another great concern to the CdS-based photocatalysts is the toxicity of leached Cd^{2+} ions [6]. Therefore, It is vitally important to develop a suitable process to inhibit the photocorrosive damage to the CdS NPs, including using sacrificial reagents, altering the structure of CdS, combining CdS with other kinds of semiconductors, adding co-catalysts to CdS, depositing a thin CdS layer on the support, and so on [4a,7–10]. The use of Na_2S and Na_2SO_3 as electron donor for CdS in photocatalytic water splitting has been considered as one of the important methods to improve the stability of CdS. however, how to reasonably conduct the compositional and structural design to achieve both high photocatalytic activity and stability in the absence of common electron donor Na_2S and/or Na_2SO_3 is still a big challenge.

Zeolite crystals with intrinsic microporosity have been widely used in industry as heterogeneous solid acid catalysts. However,

* Corresponding authors at: Shanghai Institute of Ceramics, Chinese Academy of Sciences, State Key Laboratory of High performance Ceramics and Superfine Microstructures, 1295 Dingxi Road, Shanghai 200050, PR China.
Tel.: +86 2152412706.
E-mail addresses: hrchen@mail.sic.ac.cn (H. Chen), jlshi@mail.sic.ac.cn (J. Shi).

0926-3373/$ – see front matter © 2014 Elsevier B.V. All rights reserved.
http://dx.doi.org/10.1016/j.apcatb.2014.01.024

relatively small sizes of micropores in zeolites such as Beta, ZSM-5, and TS-1 are greatly unfavorable to mass transport to/from the active sites located within them, leading to the unsatisfactory catalytic performances of zeolite catalysts [11]. Therefore, to overcome the problem, the idea of hierarchically porous zeolite has been proposed in recent years, which opens up a new way for the development of heterogeneous catalysts [12,13]. The mesoporosity of such materials can greatly facilitate the mass transport of guest species through the interconnected meso–micropore networks, and the high surface area and pore volume of mesoporous zeolites are also beneficial to the high dispersity of guest species [13]. Therefore, the hierarchically porous zeolites are much more efficient and favorable solid acid catalysts than traditional microporous zeolites for various catalytic reactions [13].

Herein, we have synthesized a mesoporous zeolite Beta using tertraethylammonium hydroxide (TEAOH) as structural directing agent and common surfactants cetyltrimethyl ammonium bromide (CTAB) as mesopore template *via* a facile solution route. Both CdS and Pt NPs were homogeneously anchored into the mesopore channels of hierarchical porous zeolite Beta to obtain highly efficient and stable Pt/CdS loaded mesoporous Beta photocatalyst (named as Pt/CdS-mBeta) for H_2 evolution by water splitting for the first time. This novel photocatalyst has the following distinctive advantages, (i) mesoporous Beta serving as catalyst matrix is beneficial to the high dispersity of CdS and Pt NPs, and the zeolite framework is well known to contain abundant electron trapping sites which are capable of transferring electrons to strong acceptors [14]; (ii) both CdS and Pt NPs can be anchored and highly dispersed into the mesopore channels due to the presence of abundant cation ions and –OH groups in mesopore channels, and the rigid aluminosilicate framework can protect CdS NPs from photocorrosion; (iii) the highly dispersed CdS and Pt NPs will be in effective contact with each other within the mesopore channels due to the confinement effect of mesopore structure, which greatly promoted the separation and migration of photogenerated charges. Rational design and fabrication of the typical hierarchically porous structure Beta is therefore demonstrated to be an attractive strategy for developing an efficient photocatalyst for H_2 evolution by water splitting under sunlight irradiation.

2. Experimental

2.1. Chemicals and reagents

Tetraethyl ammonium hydroxide(TPAOH) and cetyltrimethyl ammonium chloride (CTAB) were obtained from Shanghai J&K, China.

2.2. The synthesis of samples

2.2.1. Preparation of the mesoporous beta (mBeta)

First, 0.05 g NaCl and 0.15 KCl were dissolved into 20 mL of distilled water to obtain a homogeneous solution. Subsequently, 14.4 g of tetrapropyl ammonium hydroxide (TPAOH, 25 wt%) and 10.4 g TEOS (50 mmol) were added into the resultant solution and stirred at 313 K for 30 min. Second, the solution containing 0.162 g $NaAlO_2$ (2 mmol) was added into the resultant solution and was further stirred to obtain a emulsion at 313 K for 4 h. Finally, the emulsion was added into 5 mL aqueous solution including 1 g of cetyltrimethyl ammonium chloride (CTAB), and the reaction medium was stirred and aged for 8 h at 353 K. Afterward mesoporous Beta was obtained by hydrothermal treatment at 423 K for 24 h, after that, the products were washed with distilled water and dried at 373 K. The final products were obtained after calcination at 823 K for 8 h to remove any organics.

2.2.2. Preparation of the CdS mesoporous beta (CdS-mBeta)

0.5 M cadmium acetate dihydrate ($Cd(OAc)_2{\cdot}2H_2O$) was dissolved in 25 mL mixture solution (H_2O:EtOH = 4:1) to form a homogeneous solution, and then 0.5 g mesoporous Beta sample was added into the solution for exchanging 5 h and ion-exchanged three times at 353 K. After that, the sample was washed with deionized water by centrifugation and then dried at 373 K overnight. Then, the obtained Cd-mBeta was added into 25 mL mixture solution (H_2O:EtOH = 4:1) including 0.5 M thiourea adopted as the S source and stirred for 6 h at 353 K. The product finally was washed with deionized water by centrifugation and then dried at 373 K overnight. Finally, the CdS-mBeta was synthesized after calcination at 823 K in N_2 for 6 h.

2.2.3. Preparation of the Pt/CdS mesoporous beta (Pt/CdS-mBeta)

Varying amounts of APTES (0.5 mL, 1 mL, 2 mL and 3 mL) were separately added into 20 mL ethanol including 0.5 g CdS mesoporous Beta and stirred for 12 h at 353 K. After washing and centrifugation, the collected sample was separately re-dispersed into 20 mL $HPtCl_4{\cdot}6H_2O$ solution (0.05 M) and stirred for 2 h at 353 K. The mixture was centrifuged and washed three times with water and then dissolved into 20 mL distilled water, then the $NaBH_4$ solution (0.02 M) was added into the resultant solution dropwise until the color of the mixture changed from white to gray. After washing and centrifugation, the sample was dried overnight at 373 K and the Pt(n)/CdS-mBeta (n = 0.3, 0.6, 1.0 and 1.2) with varying amounts of the Pt NPs was formed by using a thermal treatment process at 723 K for 6 h in N_2. For comparison, the reference Pt/CdS-mBeta in the absence of APTES was obtained by a direct impregnation route, *i.e.*, CdS-mBeta was directly dispersed into 20 mL $HPtCl_4{\cdot}6H_2O$ solution (0.05 M) under stirring for 2 h at 353 K, and afterwards added into 20 mL distilled water after centrifugation and washing with water, and finally be reduced in the $NaBH_4$ solution (0.02 M) to obtain Pt/CdS-mBeta without APTES used.

2.2.4. Preparation of the Pt/CdS Al-MCM-41

The synthesis of Al-MCM-41 was carried out in a conventional hydrothermal system with a molar composition of $12NH_4OH{:}50SiO_2{:}Al_2O_3{:}8.5CTAB{:}1200H_2O$. First, aluminum isopropoxide was dissolved in deionized water, and then ammonia hydroxide and CTAB were added to the above solution. Second, TEOS was added to the mixture under strongly stirring. Afterward, mesoporous MCM-41 was synthesized by hydrothermal treatment at 393 K and then was dried at 333 K. The final products were obtained after calcination at 823 K for 8 h and named as Al-MCM-41. The Cd/Al-MCM-41was prepared by a simple impregnating method, as described briefly as follows: 0.1 M and 0.5 M cadmium acetate dihydrate ($Cd(OAc)_2{\cdot}2H_2O$) was separately dissolved in 25 mL mixture solution (H_2O:EtOH = 4:1) to form a homogeneous solution, and then the prepared 0.5 g Al-MCM-41 sample was added into the solution for impregnating for 10 h. After that, the sample was washed with deionized water by centrifugation and then dried at 373 K overnight. Next, the processes of the sulfurized treatment and the modifying of metal Pt were identical to the previous process. Finally, the samples Pt/CdS Al-MCM-41 with different CdS amounts were obtained.

2.2.5. Preparation of Pt/CdS

The CdS nanoparticles were prepared as follows: 1 mmol cadmium acetate dihydrate ($Cd(OAc)_2{\cdot}2H_2O$) and 1 mmol thiourea were separately dissolved in 20 mL H_2O solution. Then, the thiourea solution was added slowly into the $Cd(OAc)_2{\cdot}2H_2O$ solution under vigorous stirring to obtain a homogeneous solution. Next, the obtained solution was transferred to a Teflon-lined stainless steel autoclave and heated at 433 K for 24 h (hydrothermal treatment).

The final solid CdS nanoparticles can be obtained after filtering, washing with water and ethanol 4–5 times, and then dried at 353 K for 12 h. Next, H_2PtCl_6 aqueous solution (0.005 M) was added to a suspension of prepared CdS (1 g) in acetic acid (AcOH, 50 mL, 0.25 M). The mixture was irradiated with 500 W Xe lamp for 60 min. The resulting suspension was filtered, washed with water, and dried at 363 K to obtain Pt/CdS.

2.3. Characterization

Powder X-ray diffraction (XRD) patterns were recorded on a Rigaku D/Max 2200PC diffractometer using Cu $K\alpha$ radiation (40 kV and 40 mA) with a scanning rate of 4°/min for high angle tests. The nitrogen sorption measurements were performed using Micromeritics Tristar 3000 and Micromeritics ASAP 2020 porosimeters at 77 K; the mesoporous specific surface area and the pore size distribution were calculated using the Brunauer–Emmett–Teller (BET) and Barrett–Joyner–Halenda (BJH) methods, respectively. Transmission electron microscopic (TEM) imaging and selected area electron diffraction (SAED) and EDS were performed on a JEOL-2010F electron microscope operated at 200 kV, while FE-SEM (Field Emission Scanning Electron Microscope) images were obtained on Hitachi S-4800. The acidic property of samples were obtained by temperature programmed desorption of ammonia (NH_3-TPD). The content of metal CdS and Pt were measured using inductively coupled plasma atomic emission spectroscopy (ICP–AES) analyzer on a Vista AX. The UV–Vis absorption spectra were recorded using a UV-3101PC Shimadzu spectroscope. Fourier transform infrared (FTIR) spectra were obtained in the range of 400–4000 cm^{-1} using a Nicolet 7000-C instrument.

2.4. Electrode preparation for PEC measurements

FTO of 1.25 cm^2 served as substrate for the catalyst materials. Catalyst ink with 5 mg/mL (EtOH:water = 1:1, volume scale) and 25 μL Nafion solution (5%) was dispersed ultrasonically, and then 1 mL mixture was transferred onto the FTO substrate.

2.5. Photoelectrochemical measurements

Photoelectrochemical measurements were conducted using a normal three-electrode system cell. Prepared photoelectrode, Pt wire, and Ag/AgCl electrode were used as a working, counter, and reference electrode. 0.1 M Na_2SO_4 aqueous solution was employed as an electrolyte. 300 W Xe lamp was employed as a light source. For photocurrent–voltage (J–V) curve measurement, the potential of specimen was swept to positive direction with a rate of 10 mV/s under sunlight irradiation.

2.6. Photocatalytic H_2 evolution

The photocatalytic activities of the samples were examined in a gas-closed system. A catalyst sample of 100 mg was dispersed in 200 mL of deionized water and 20 mL ethanol in a glass reactor. The photoreaction system was purged with high-purity argon for 30 min to remove air. The light source was a 500 W Xe lamp. The reaction proceeded under vigorous stirring. The evolved H_2 gas was determined with on-line gas chromatography equipped with a thermal conductivity detector (TCD).

3. Results and discussion

3.1. The synthesis of Pt/CdS NPs co-loaded mesoporous beta

Mesoporous Beta was successfully synthesized by using a common surfactant CTAB, rather than cationic polymers [15], as a mesopore template, and Pt/CdS NPs-co-loaded hierarchically porous zeolite Beta can be synthesized through a facile successional two-step pore modification technology. Since there are many cationic ions ($R = Na^+$, K^+, H^+ and Al^{3+}) and –OH groups present on the mesopore channels of the hierarchically porous Beta, the CdS and Pt NPs can be easily anchored in the mesopore channels by the ion-exchange process and strong coordination ability between Pt precursors and amino groups of APTES, as shown in Scheme 1. First, cadmium acetate dihydrate ($Cd(OAc)_2{\cdot}2H_2O$) and thiourea were adopted as Cd and S sources, respectively, and the Cd^{2+} ions were firstly incorporated in mesopore channels by an ion-exchange method, thus the highly dispersed CdS NPs could form within the mesopore channels by the follow-up sulfurization (Scheme 1 step I). Second, the abundant –OH groups presented in mesopore channels would react with the amino groups of introduced APTES, and the formed NH_4^+ of APTES could strongly coordinated with $PtCl_4^-$ of the introduced $H_2PtCl_4{\cdot}6H_2O$ at 353 K, thus the highly dispersed Pt NPs could be *in situ* generated within the mesopore channels through the reduction by $NaBH_4$ (Scheme 1 step II). Finally, CdS and Pt NPs co-loaded mesoporous Beta with high dispersion and close contact was obtained based on the confinement effect of mesopore channels.

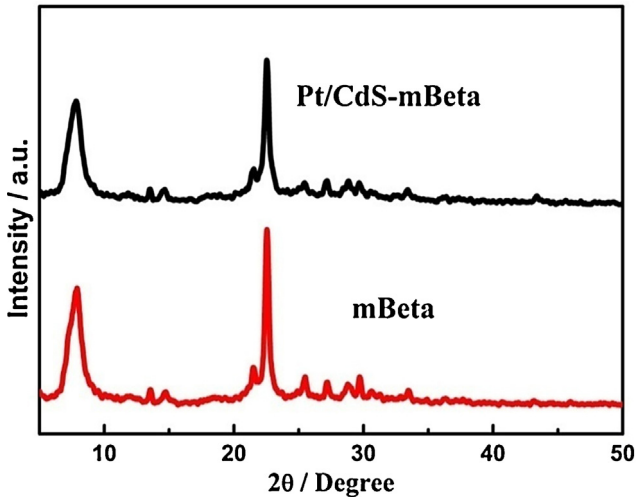

Fig. 1. XRD patterns of the samples mBeta and Pt/CdS-mBeta.

3.2. Structural characterization

The X-ray diffraction (XRD) patterns of mesoporous Beta (mBeta) and Pt/CdS-mBeta (Fig. 1) show well-resolved diffraction peaks of the zeolite Beta structure in the 5–50° range, and no diffraction peaks corresponding to CdS or Pt NPs can be detected in the Pt/CdS-mBeta, suggestive of high dispersity of both CdS and Pt NPs within the mesoporous zeolite beta. Interestingly, N_2 adsorption/desorption isotherms (Fig. 2a) of both mBeta and Pt/CdS-mBeta exhibit significant steps at a relative pressure $P/P_0 = 0.45$, confirming the presence of mesopore structure with well defined pore size distribution in both samples, also implying the highly dispersity of Pt/CdS species. In addition, a slight increase at $P/P_0 = 0.95$ indicates the presence of a larger interparticle porosity. Correspondingly, the pore size distributions for both mBeta and Pt/CdS-mBeta demonstrate that mesopores are mainly distributed in 3–10 nm (Fig. 2b), and the BET surface areas and total pore volumes of the two samples were calculated to be 689 m^2/g, 0.52 cm^3/g and 617 m^2/g, 0.45 cm^3/g, respectively. It is clear that the surface area and total pore volume of the prepared Pt/CdS-mBeta show only slight decreases after Pt/CdS loading (Table 1), indicative of the

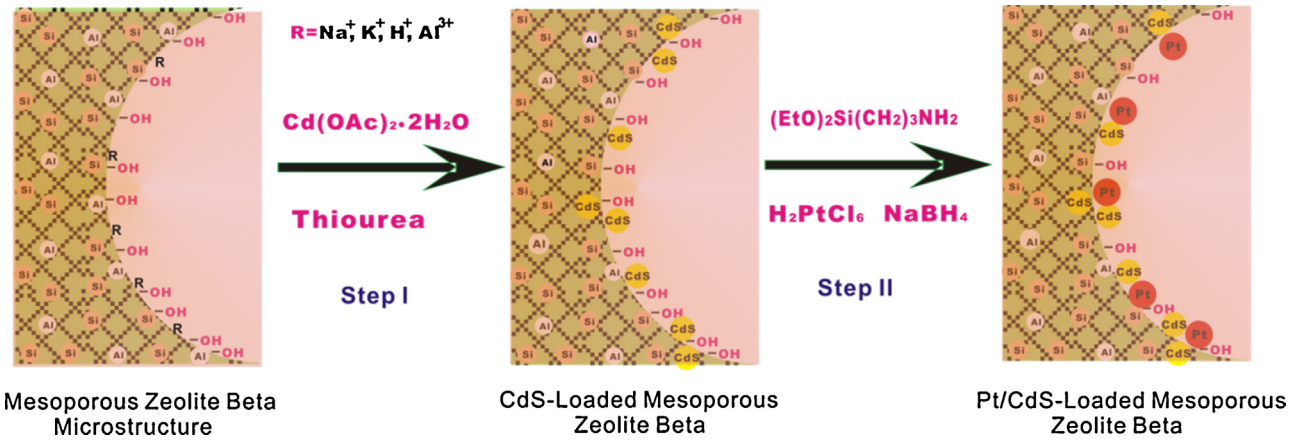

Scheme 1. Schematic drawing of the formation mechanism of sample Pt/CdS-mBeta. Step I: The CdS NPs were incorporated in mesopore channels of hierarchically porous zeolite Beta by an ion-exchange method. Step II: The Pt NPs in the mesopore channels are *in situ* generated *via* complexation by grafted amino groups and the subsequent reduction by $NaBH_4$.

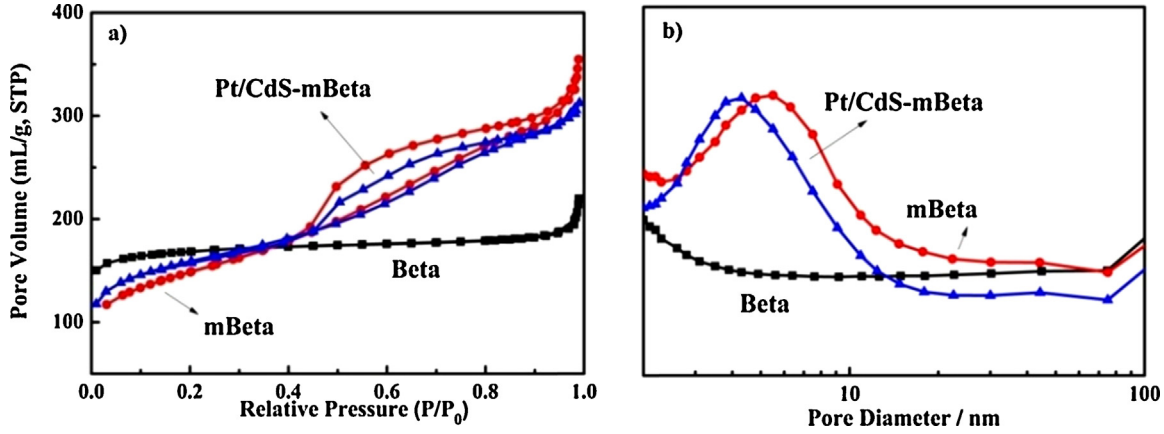

Fig. 2. (a) N_2 adsorption/desorption isotherms and (b) corresponding BJH pore diameter distribution curves of the samples Beta, mBeta and Pt/CdS-mBeta.

unblocked mesopore channels due to the high dispersity of Pt/CdS species of extremely small sizes.

The field emission scanning electron microscopic (FE-SEM) image of the prepared Pt/CdS-mBeta in Fig. 3a reveals the predominant presence of uniformly sized particles with similar quasi-spherical morphology, suggestive of the nearly pure phase of mesoporous zeolite of the synthesized sample. The high-magnification FE-SEM image in Fig. 3b clearly shows the interesting nanoarchitecture of a mesoporous zeolite particle with well-defined and uniform mesopore structure interpenetrating the zeolite crystals. The high resolution transmission electron microscope TEM (HR-TEM) image (Fig. 4a, left) clearly shows the lattice

Table 1
Texture properties and the H_2 evolution rates over various catalysts.

Sample	S_{BET}[a] (m^2/g)	V_{total}[b] (cm^3/g)	CdS[c] (wt%)	Pt[c] (wt%)	H_2 evolution[d] (mmol/$g_{catalyst}$/h)	H_2 evolution[d] (mmol/g_{CdS}/h)	Sacrificial agent
mBeta	689	0.52	–	–	–	–	–
CdS-mBeta	650	0.48	1.5	–	0.18	12	Ethanol
Pt/CdS	–	–	99.0	1.0	4.34	4.44	Ethanol
Pt/CdS-mBeta	617	0.45	1.5	1.0	3.09	206	Ethanol
Pt/CdS-mBeta	617	0.45	1.5	1.0	~0	~0	–
Pt/CdS-mBeta[e]	617	0.45	1.5	1.0	1.56	104	Ethanol
Pt/CdS Al-MCM-41	826	0.78	15.6	1.0	1.93	12	Ethanol
Pt/CdS Al-MCM-41	826	0.78	1.5	1.0	1.68	113	Ethanol
RuO_2-CdS-Ti-MCM-48 [1]	797	0.58	–	–	0.26	–	Ethanol
CdS-Ti-MCM-48 [1]	1139	0.66	–	–	2.73	–	Ethanol
Pt/ZrO_2/TaON [2]	–	–	–	1.0	0.52	–	NaI
g-C_3N_4 nanosheets [3]	384	–	–	3.0	1.86	–	Triethanolamine
GC(1.0) [4]	48.2	–	99	0.5	56.00	57	Lactic acid

[a] S_{BET} is the BET surface area.
[b] V_{total} is the single-point adsorption total pore volume at $P/P_0 = 0.984$.
[c] The contents of the CdS and Pt are determined by ICP–AES analysis.
[d] Reaction condition: 0.1 g catalyst, 200 mL H_2O, 20 mL C_2H_5OH, 500 W Xe lamp.
[e] Pt was loaded in the CdS-mBeta in the absence of APTES Refs. [1–4].

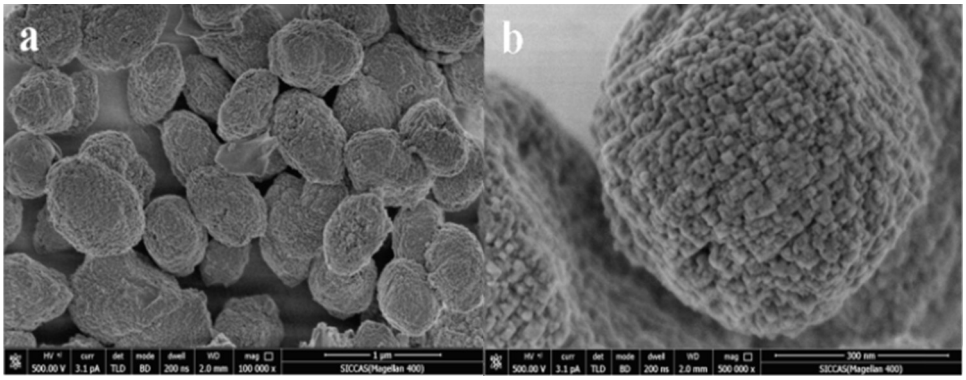

Fig. 3. (a) Low and (b) high-magnification FE-SEM images of the sample Pt/CdS-mBeta.

fringes of zeolite beta and the corresponding selected area electron diffraction (SAED) pattern in the inset of Fig. 4a confirms that the prepared Pt/CdS-mBeta has a single crystalline character. More importantly, the corresponding elemental analysis by energy dispersive spectroscope (EDS) (Fig. 4a, right) indicates the co-presence of Cd, S and Pt (as shown in arrows) in this sample. Furthermore, the STEM images and the corresponding element mappings of the prepared sample in Fig. 4b confirm that CdS (1.5 wt%) and Pt NPs (1.0 wt%) are highly dispersed in the mesoporous zeolite, and no CdS aggregates and/or large Pt particles can be found in the sample Pt/CdS-mBeta, further confirming the presence of highly dispersed CdS and Pt NPs confined within the hierarchically porous structure of zeolite matrix.

The UV–Vis spectra for the references mBeta and CdS-mBeta, and the prepared Pt/CdS-mBeta, are shown in Fig. 5 for comparison. It is clear that compared to mBeta, the reference CdS-mBeta shows an enhanced absorbance in the visible-light region, confirming that CdS NPs are capable of absorbing visible light. The Pt/CdS-mBeta displays two absorption bands at 217 nm and 575 nm, which can be assigned to the absorption by Pt and CdS NPs, respectively. More importantly, the Pt/CdS-mBeta shows a blue shift approximately by 25 nm compared to the bulk CdS particles (~600 nm) [8] due to the quantum size effect of CdS NPs, further confirming the successful encapsulation of CdS NPs inside the mesopore channels. The result of NH_3-TPD (Fig. S1 and Table S1) indicates that Pt/CdS-mBeta has a higher total acid amount (0.82 mmol-NH_3/g) than that of the reference Pt/CdS Al-MCM-41 (0.63 mmol-NH_3/g) due to the higher Al content in crystalline Beta zeolite framework. In addition to the desorption peak at around 100 °C corresponding to the weak acidic sites for both Pt/CdS-mBeta and Pt/CdS Al-MCM-41 samples, Pt/CdS-mBeta also possesses a distinct weak desorption peak at about 550 °C, which can be attributed to the

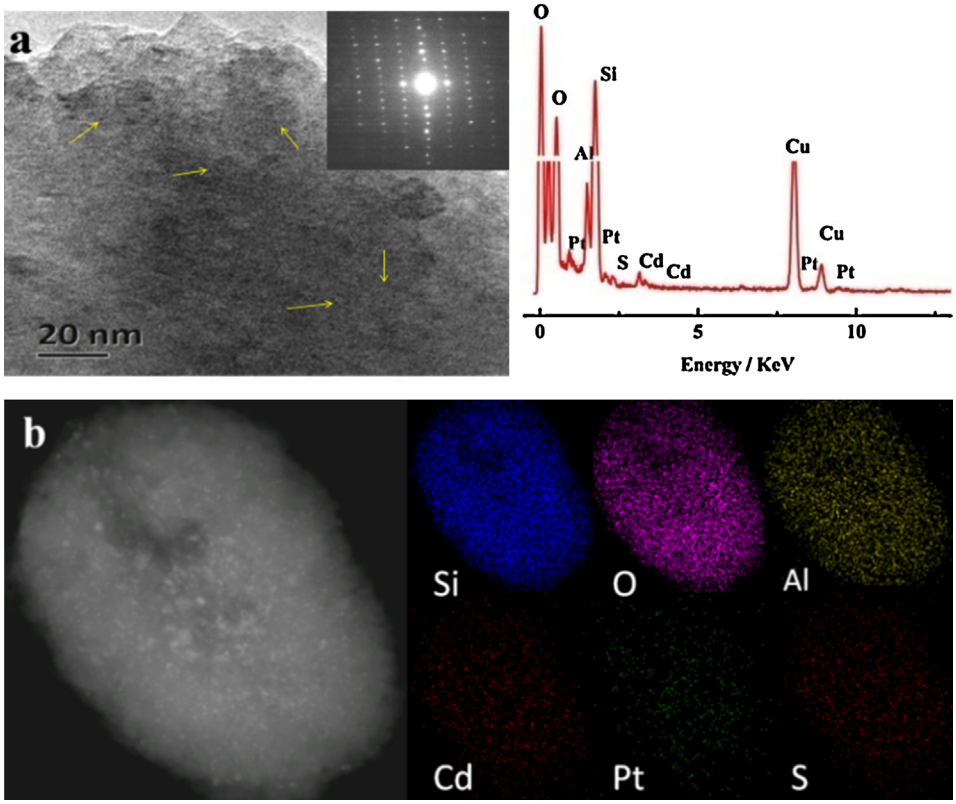

Fig. 4. (a) Typical HR-TEM image (left) of the sample Pt/CdS-mBeta (yellow arrows indicate CdS and Pt NPs) and the corresponding selected area electron diffraction (SAED) pattern (inset) and EDS spectrum (right) of the designated area in Pt/CdS-mBeta; (b) STEM images and the corresponding element mappings of the sample Pt/CdS-mBeta. (For interpretation of the references to color in this figure legend, the reader is referred to the web version of this article.)

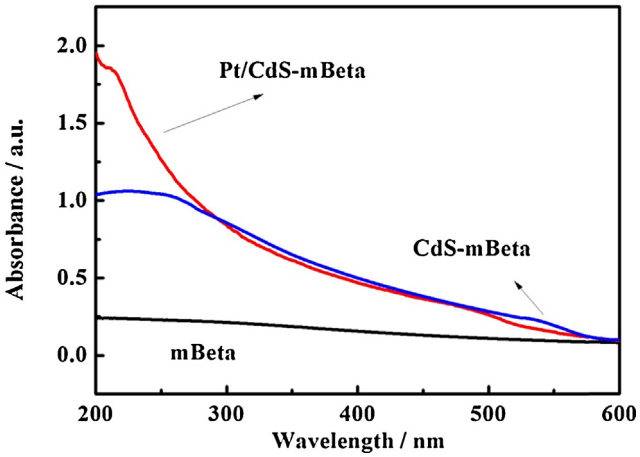

Fig. 5. UV–Vis spectra of the samples mBeta, CdS-mBeta and the Pt/CdS-mBeta.

strong acidic sites related to Al sites in the crystalline Beta framework [16].

3.3. H_2 evolution by water splitting under sunlight irradiation

Fig. 6 shows the photocurrent–voltage curves of the prepared Pt/CdS-mBeta and the references CdS-mBeta and Pt/CdS Al-MCM-41 deposited on modified FTO substrates in 0.1 M Na_2SO_4 electrolyte. It can be found that the CdS-mBeta yields a relatively low photocurrent density of 0.34 mA/cm^2 at 1.23 V *vs* NHR (normal hydrogen electrode), but the photocurrent density of the Pt/CdS-mBeta remarkably increased by a factor of 55, reaching 18.8 mA/cm^2 at 1.23 V *vs* NHR. The photocurrent density and onset potential are greatly enhanced after Pt introduction due to the electron migration from CdS to Pt NPs and the formation of Schottky barrier, as an electron trap, at the interface between Pt and CdS NPs, which will greatly promote the transfer and separation of photoinduced electrons and holes, thus enhancing its electrochemical activity. Besides, the Pt/CdS-mBeta also shows a much higher electrochemical activity than the reference Pt/CdS Al-MCM-41, which is attributed to the crystalline zeolitic framework of the former. The zeolite matrix with higher acid content can stabilize electrons separated from the electron–hole pairs in the zeolite framework and then transfer the electrons to the strong acceptors of zeolite [14],

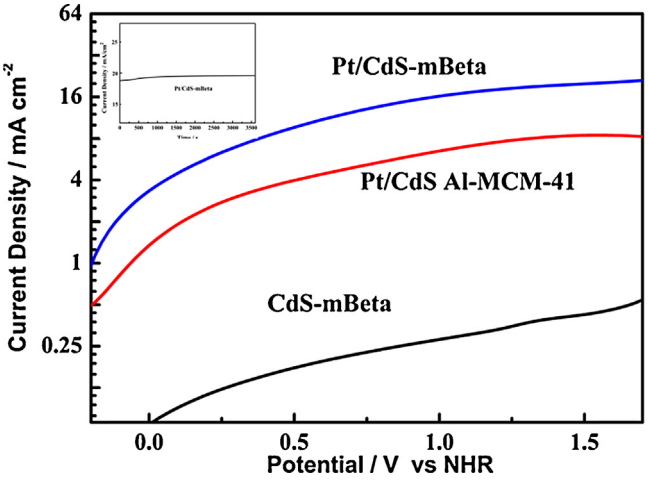

Fig. 6. Photocurrent–voltage curves of samples CdS-mBeta, Pt/CdS-mBeta and Pt/CdS Al-MCM-41 electrodes deposited on FTO substrates, and the time dependence of catalytic currents (inset) during the electrolysis of CdS/Pt-mBeta at an applied potential of +1.23 V *vs* NHR (0.1 M Na_2SO_4(aq), 300 W Xe lamp).

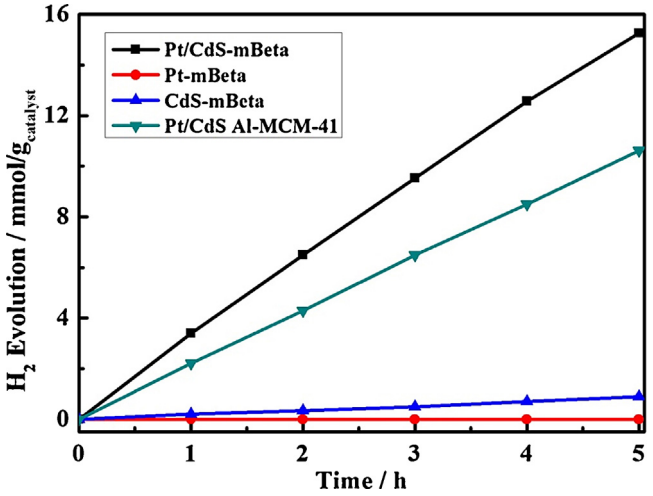

Fig. 7. Photocatalytic H_2 evolutions over the different samples CdS-mBeta, Pt/CdS-mBeta, Pt-mBeta and Pt/CdS Al-MCM-41 (0.1 g catalyst, 200 mL H_2O, 20 mL C_2H_5OH, 500 W Xe lamp).

effectively preventing the recombination of the photogenerated charges and elevating its electronchemical activity. In addition, the photocurrent from the Pt/CdS-mBeta electrode is stable and no observable decay can be found during 60 min in 0.1 M Na_2SO_4 (inset in Fig. 6), indicative of the excellent stability of the Pt/CdS-mBeta.

Fig. 7 shows the results of photocatalytic H_2 evolution rates over the samples CdS-mBeta, Pt/CdS-mBeta, Pt/CdS Al-MCM-41 and Pt-mBeta with same Pt-loading or/and CdS-loading for comparison. It is clear that the Pt/CdS-mBeta exhibits the highest H_2 evolution rate (3.09 mmol/h/$g_{catalyst}$) compared to the references Pt/CdS Al-MCM-41 and CdS-mBeta, while Pt-mBeta cannot generate any H_2 under the same condition. The above results indicate that the pure Pt NPs are catalytically inactive for the H_2 evolution *via* water splitting in the reaction system, while CdS NPs are considered as the main active centers. Very interestingly, the prepared CdS/Pt co-loaded mesoporous Beta sample exhibits a greatly enhanced photocatalytic activity, which could most probably be attributed to the synergetic catalytic effect occurring at the interfaces between CdS and Pt, or among CdS, Pt and the Beta matrix.

More importantly, this novel photocatalyst also shows much superior H_2 evolution performance to those of the previous reports [8,10,17], as shown in Table 1. Compared to the reported RuO_2-CdS-Ti-MCM-48 and CdS-Ti-MCM-48 samples [8] and the reference Pt/CdS Al-MCM-41, our prepared Pt/CdS-mBeta shows lower surface area but much enhanced catalytic H_2 evolution rate *via* water splitting, implying the existence of possible synergetic effects between CdS and Pt components. More significantly, the mesoporous zeolite Beta carrier with high acid density can stabilize electrons and accelerate the separation of photogenerated electrons and holes, thus greatly improving the photocatalytic activity of the sample Pt/CdS-mBeta, which will be discussed in detail in the following section. Besides, the Pt/CdS-mBeta (206 mmol/h/g_{CdS}, CdS, 1.5 wt%) and Pt/CdS Al-MCM-41 (113 mmol/h/g_{CdS}, CdS, 1.5 wt%) samples with mesoporous structured supports exhibit much higher H_2 evolution rate than reference samples CdS/GC (57 mmol/h/g_{CdS}, CdS, 99 wt%) and Pt/CdS (4.44 mmol/h/g_{CdS}, CdS, 99 wt%) without porous support, which suggests that the mesostructured catalyst carrier with large BET surface area facilitates the high dispersity of CdS and Pt NPs, thus greatly increasing the photocatalytic activity for H_2 evolution. Moreover, it can be found that H_2 evolution rate decreases with the increase of CdS-loading amounts on Pt/CdS Al-MCM-41 (Table 1), *i.e.*, Pt/CdS Al-MCM-41 with a higher CdS-loading amount (15.6 wt%, H_2,

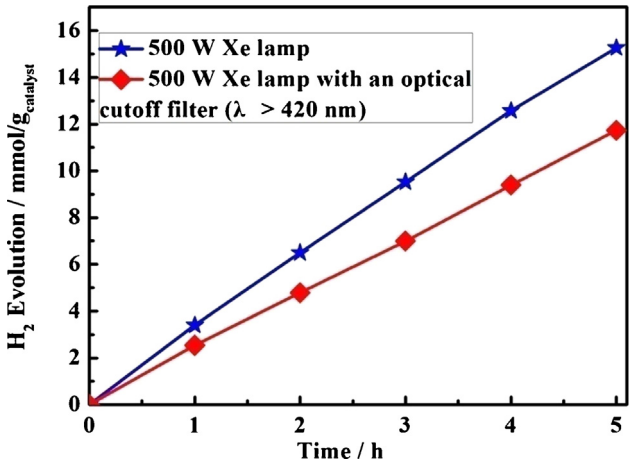

Fig. 8. Photocatalytic H_2 evolutions over the sample Pt(1.0)/CdS-mBeta under light radiations of different wavelengths (0.1 g catalyst, 200 mL H_2O, 20 mL C_2H_5OH, 500 W Xe lamp).

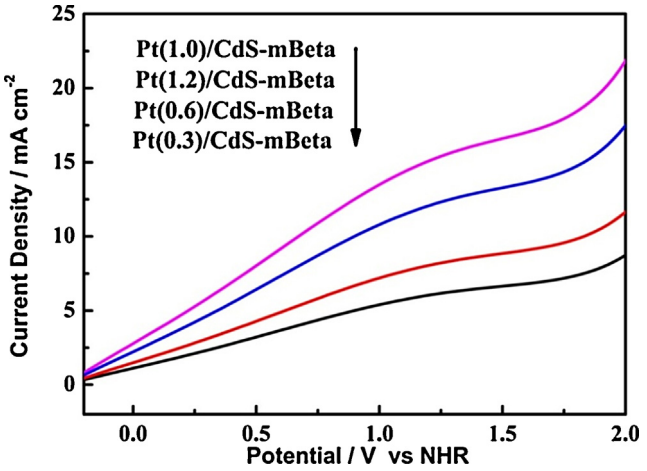

Fig. 9. Photocurrent–voltage curves for the Pt/CdS-mBeta electrodes with varying contents of the Pt NPs deposited on FTO substrates (0.1 M Na_2SO_4(aq), 300 W Xe lamp, 10 mV/s).

12 mmol/h/g_{CdS}) shows a lower H_2 evolution rate than that with low CdS-loading amount (1.5 wt%, H_2, 113 mmol/h/g_{CdS}), meaning that the excess CdS-loading amount can lead to the formation of CdS aggregates, and thus lead to the decreased photocatalytic activity.

It should be noted that the photocatalyst Pt/CdS-mBeta itself is unable to produce H_2 from pure water in the absence of sacrificial agent (Table 1). In this photocatalytic reaction system, due to the recombination of the produced holes and electrons in pure water, it is important to introduce sacrificial agent as electron donors to consume the produced holes and promote the H_2 evolution rate. Herein, the C_2H_5OH solution was used as sacrificial agent to act as a consumer of photoinduced holes.

In order to explore the origin of H_2 production, the phocatalytic activities of the sample Pt/CdS-mBeta in different reaction systems were measured and the results are shown in Fig. S2. In the presence of common sacrificial agent Na_2S and Na_2SO_3, no hydrogen can be detected from the pure C_2H_5OH solution while a considerable amount of H_2 evolution can be achieved in the pure H_2O solution over the sample Pt/CdS-mBeta, implying that the produce H_2 is coming from the H_2O rather than from C_2H_5OH in the mixed H_2O/C_2H_5OH solution.

The photocatalytic activity of Pt/CdS-mBeta under visible light irradiation at different wavelengths was further investigated by using 500 W xenon lamp with an optical cutoff filter ($\lambda > 420$ nm), as shown in Fig. 8. It is found that the sample Pt/CdS-mBeta still owns highly catalytic activity with 2.35 mmol/h/$g_{catalyst}$ of H_2 evolution rate even under the visible light irradiation, indicative of the high catalytic activity.

In addition, the obtained Pt species are apt to aggregate with each other in the case of using no APTES, forming large particles on the surface of sample (Fig. S3), which will lead to the decreased photocatalytic activity (Table 1). In the presence of APTES, due to the strong coordination between Pt precursors and amino groups of APTES at elevated temperatures (353 K) [18], the generated Pt NPs can be well confined into the mesopore channels, avoiding the formation of large Pt species aggregates. Therefore, it is believed that APTES plays an important role in the formation of highly dispersed Pt NPs. Moreover, the Pt(n)/CdS-mBeta with varied Pt-loading amounts can be obtained by changing the contents of APTES. Figs. 9 and 10 show photocurrent–voltage curves and the H_2 production rates obtained at the Pt(n)/CdS-mBeta. It is found that the obtained proper amount of Pt-loading owing to the optimal APTES dosage has a profound contribution to the electrochemical activity and H_2 evolution rate. Though the increase in the Pt content can promote the charge separation and thus improve the photocatalytic activity, excess amount of Pt may decrease electrochemical activity and H_2 evolution rate. This is because that excess amount of Pt NPs together with small amount of APTES can cover some active sites (CdS NPs and acid sites) and shield the sunlight and water molecules from reaching the CdS species, thus leading to the decreased H_2 evolution rate. Therefore, there is an optimized dosage of Pt in the photocatalytic reaction system.

The structural and catalytic stability is also one of the most important issues for photocatalysts. The FT-IR results of the prepared Pt/CdS-mBeta for both before and after catalytic reactions shown in Fig. S4, indicates no distinguishable changes in the structure can be found after the catalytic reaction as compared to that before the reaction. Besides, no significant Cd^{2+} leaching can be detected from the filtrate by ICP–AES analyses, indicating the strong binding between Cd^{2+} and the matrix. Fig. 11 shows the recycling performance of Pt/CdS-mBeta in the H_2 evolution *via* water splitting. Although the H_2 evolution rate of Pt/CdS-mBeta sample becomes a little lower after 7 cycle tests, probably owing to the inevitable oxidation of sulfur species, to a certain extent, by photogenerated holes under sunlight irradiation, the H_2 evolution still maintains a high rate of 2.49 mmol/h/$g_{catalyst}$ on the sample Pt/CdS-mBeta, indicative of sustainable photocatalytic activity. Those results further confirm that the designed

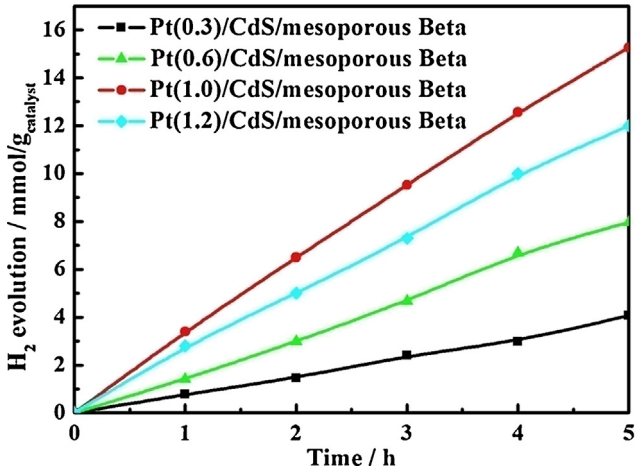

Fig. 10. Photocatalytic H_2 evolution over the sample Pt/CdS-mBeta with varying contents of the Pt NPs (0.1 g catalyst, 200 mL H_2O, 20 mL C_2H_5OH, 500 W Xe lamp).

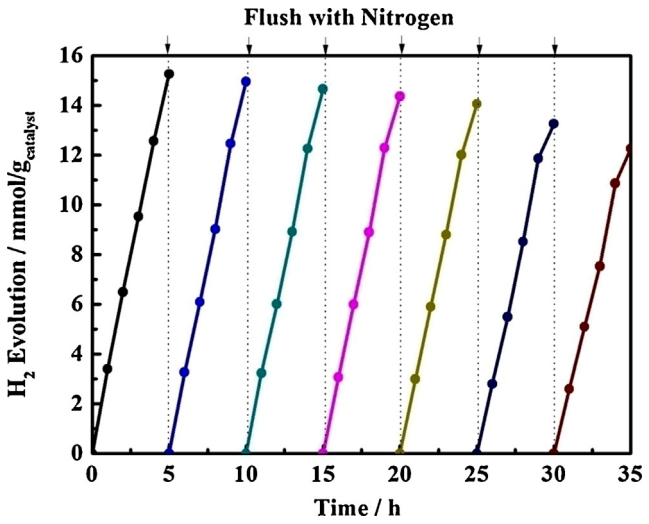

Fig. 11. Recyclability of the sample Pt/CdS-mBeta in the H_2 evolution by water splitting (0.1 g catalyst, 200 mL H_2O, 20 mL C_2H_5OH, 500 W Xe lamp).

photocatalyst Pt/CdS-mBeta has an excellent structural and catalytic stability against photocorrosion due to the strong binding between Cd ions and the matrix hierarchically porous zeolite by ion-exchange process. Additionally, This anti-photocorrosion effect can also be ascribed to the following aspects: (1) well-defined mesostructure of the hierarchically porous zeolite provides an excellent confinement effect in dispersing and stabilizing CdS NPs, thus preventing the formation of large CdS aggregates; (2) the presence of sacrificial agent C_2H_5OH as electron donors can consume the produced holes, avoiding the oxidation of sulfur species to a certain extent.

3.4. Synergetic catalytic effect

The excellent photocatalytic activity of Pt/CdS-mBeta can be ascribed to both the hierarchically porous zeolite structure and the effective contact between CdS and Pt NPs which are highly dispersed in the mesopore structure. The CdS and Pt NPs are *in situ* generated from their precursors introduced in the mesopore network and come into close contact with each other in the mesopore channels due to the confinement effect of mesopore channels. It is believed that the photogenerated electrons and holes can be effectively separated and migrated through the following two ways in this catalyst system: (1) Schottky barrier, as an electron trap, are created at the interface between n-type semiconductor CdS and metal Pt NPs, which can effectively prevent the recombination of the photogenerated electrons migrated from CdS to Pt and holes remaining on CdS, therefore, the photocurrent density and onset potential are improved dramatically with the introduction of Pt NPs; (2) more specifically, the zeolite framework with enriched acid sites can bind and immobilize photogenerated electrons from the electron–hole pairs in the zeolite framework, which can also contribute to the separation of photogenerated electrons and holes and/or retard recombination of photocharges under sunlight irradiation, and consequently increase the photocatalytic activity, as shown in Scheme 2. The interactions between CdS and Pt NPs, and between CdS and Beta matrix can be both contributed to the synergetic catalytic effect [19] *via* CdS activation (electron–hole separation and recombination prevention) by Pt NPs and Beta matrix, respectively. The former is featured with the electron sinking on Pt and the prevention of electron/hole recombination by Schottly barrier between CdS and Pt; and the latter is achieved by the electron binding on acidic Beta, *i.e.*, by positively charged acidic sites on mesopore surface, facilitating the electron–hole separation and the recombination prevention [19]. In fact, in the case of the synergetic effect between CdS and Pt NPs, the photogenerated electrons migrated to Pt can be further captured onto the acidic sites on mesopore surface of Beta matrix, which also contribute to the preventions of electron transfer back to CdS and the subsequent electron–hole recombination, as also shown in Scheme 2. Under the effective electron/hole recombination preventions by Pt and Beta matrix, the photogenerated holes produced from the Pt/CdS-mBeta can migrate to the surface of the photocatalyst and oxidize the ethanol in the solution, as shown in Scheme 2, similarly to the previous report [8] and thus enhanced H_2 evolution could be obtained in the reaction system.

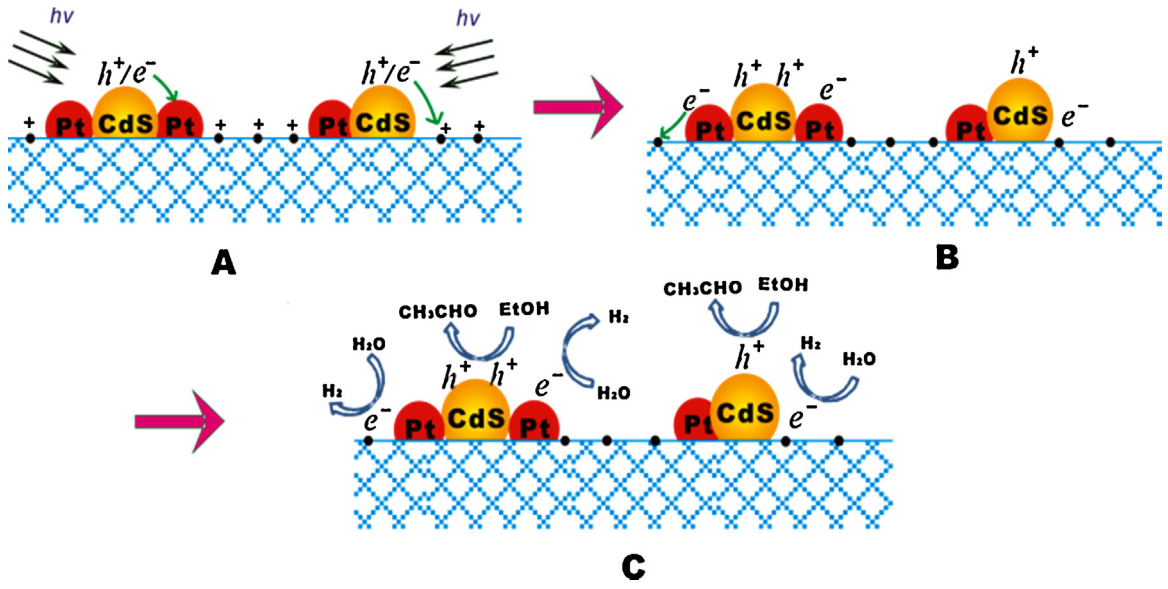

Scheme 2. Synergetic catalytic effect proposal for the enhanced H_2 evolution by water splitting on Pt/CdS-mBeta photocatalyst. (A) Formation of photogenerated electrons and holes under sunlight irradiation; (B) separations and transfers of photogenerated electrons from CdS to Pt, and possibly further to the acidic sites of Beta matrix (the left), or, from CdS directly to Beta matrix due to the binding effect of the positively charged acidic sites to the electrons (the right); (C) H_2 evolution by water splitting remarkably enhanced by the promoted electron–hole separation and recombination prevention by the synergetic effects.

4. Conclusions

In conclusion, a highly efficient and stable photocatalytic H_2 evolution from water splitting under sunlight irradiation has been achieved over the novel Pt/CdS NPs-co-loaded mesoporous Beta photocatalyst synthesized by a rational pore modification process. The CdS and Pt NPs are co-introduced and highly dispersed within the mesopore network of typical mesoporous zeolite structure, which ensure the effective and close contact between CdS and Pt species within the mesopore network. This novel Pt/CdS NPs-co-loaded mesoporous Beta photocatalyst demonstrates an extremely high photocatalytic H_2 evolution rate of 3.09 mmol/h/$g_{catalyst}$ or 206 mmol/h/g_{CdS}, even with very low CdS- (1.5 wt%) and Pt-loading (1.0 wt%) under sunlight irradiation, which can be ascribed to the efficient separation and transfer of photoelectrons and holes in this catalyst system *via* the synergetic catalytic effect between CdS and Pt NPs, and between CdS and zeolite Beta matrix. Importantly, the sample shows an excellent structural and catalytic stability due to the strong binding between CdS/Pt NPs and the matrix hierarchically porous zeolite, and additionally, the confinement effect by the mesostructured Beta support for CdS NPs and the use of sacrificial agent C_2H_5OH are also suggested contributing to the outstanding catalytic stability. Such strategies may provide opportunities for developing more kinds of high performance photocatalysts with enhanced efficiencies for solar energy conversion.

Acknowledgment

This research was sponsored by National Key Basic Research Program of China, (2013CB933200), China National Funds for Distinguished Young Scientists (51225202), National Natural Science Foundation of China (51202278, 51102172), Key Program for Science and Technology Commission of Shanghai Municipality (11JC1413400), State Key Laboratory of Heavy Oil Processing (2012-1-04) and Natural Science Foundation of Shanghai (12ZR1435200).

Appendix A. Supplementary data

Supplementary data associated with this article can be found, in the online version, at http://dx.doi.org/10.1016/j.apcatb.2014.01.024.

References

[1] (a) K. Maeda, K. Teramura, D.L. Lu, T. Takata, N. Saito, Y. Inoue, K. Domen, Nature 440 (2006) 295;
(b) H.G. Kim, D.W. Hwang, J.S. Lee, J. Am. Chem. Soc. 126 (2004) 8912;
(c) M. Gratzel, Nature 414 (2001) 338;
(d) X.B. Chen, L. Liu, P.Y. Yu, S.S. Mao, Science 331 (2011) 746;
(e) A. Kudo, Y. Miseki, Chem. Soc. Rev. 38 (2009) 253;
(f) F.E. Osterloh, Chem. Mater. 20 (2008) 35;
(g) R.M. Navarro, M.C. Sanchez-Sanchez, M.C. Alvarez-Galvan, F. Valle, J.L.G. Fierro, Energy Environ. Sci. Rev. 2 (2009) 35.
[2] J. Kim, D.W. Hwang, H.G. Kim, J.S. Lee, W. Li, S.H. Oh, Top. Catal. 35 (2005) 295.
[3] H. Kato, K. Asakura, A. Kudo, J. Am. Chem. Soc. 125 (2003) 3082.
[4] (a) M.D.H. Alonso, F. Fresno, S. Suarez, J.M. Coronado, Energy Environ. Sci. 2 (2009) 1231;
(b) M. Matsumura, S. Furukawa, Y. Saho, H. Tsubomura, J. Phys. Chem. 89 (1985) 1327;
(c) J. Reber, F.M. Rusek, J. Phys. Chem. 90 (1986) 824.
[5] (a) D. Meissner, R. Memming, B. Kastening, J. Phys. Chem. 92 (1998) 3476;
(b) D.N. Ke, S.L. Liu, K. Dai, J.P. Zhou, L.N. Zhang, T.Y. Peng, J. Phys. Chem. C 113 (2009) 16021.
[6] Y. Hu, X. Gao, L. Yu, Y. Wang, J. Ning, S. Xu, X. Wen (David) Lou, Angew. Chem. Int. Ed. 52 (2013) 1.
[7] (a) R. Peng, D. Zhao, J. Baltrusaitis, C.M. Wu, R.T. Koodali, RSC Adv. 2 (2012) 5754;
(b) S.Y. Ryu, W. Balcerski, T.K. Lee, M.R. Hoffmann, J. Phys. Chem. 111 (2007) 18195.
[8] R. Peng, C.M. Wu, J. Baltrusaitis, N.M. Dimitrijevic, T. Rajhcan, R.T. Koodali, Chem. Commun. (2013), http://dx.doi.org/10.1039/b000000x.
[9] M. Moriya, T. Minegishi, H. Kumagai, M. Katayama, J. Kubota, K. Domen, J. Am. Chem. Soc. (2013), http://dx.doi.org/10.1021/ja312653y.
[10] Q. Li, B. Guo, J. Yu, J. Ran, B. Zhang, H. Yan, J. Gong, J. Am. Chem. Soc. 133 (2011) 10878.
[11] (a) M.E. Davis, Nature 417 (2002) 813;
(b) M. Hartmann, Angew. Chem. 116 (2004) 6004, 116;
(c) M. Hartmann, Angew. Chem. Int. Ed. 43 (2004) 5880.
[12] (a) J. Aguado, D. Serrano, J. Rodriguez, Microporous Mesoporous Mater. 115 (2008) 504;
(b) F.S. Xiao, L. Wang, C. Yin, K. Lin, Y. Di, J. Li, R. Xu, D.S. Su, R. Schlögl, T. Yokoi, Angew. Chem. Int. Ed. 118 (2006) 3162;
(c) J.C. Groen, W. Zhu, S. Brouwer, S.J. Huynink, F. Kapteijn, J.A. Moulijn, J. Pérez-Ramírez, J. Am. Chem. Soc. 129 (2007) 355;
(d) Z. Yang, Y. Xia, R. Mokaya, Adv. Mater. 16 (2004) 727;
(e) L.H. Chen, X.Y. Li, G. Tian, Y. Li, J.C. Rooke, G.S. Zhu, S.L. Qiu, X.Y. Yang, B.L. Su, Angew. Chem. Int. Ed. 50 (2011) 11156.
[13] (a) Z.L. Hua, J. Zhou, J.L. Shi, Chem. Commun. 47 (2011) 10536;
(b) Y. Song, Z. Hua, Y. Zhu, J. Zhou, X. Zhou, Z. Liu, J. Shi, J. Mater. Chem. 22 (2012) 3327;
(c) J. Zhao, J. Zhou, Y. Chen, Q. He, M. Ruan, L. Guo, J. Shi, H. Chen, J. Mater. Chem. 19 (2009) 7614;
(d) J. Zhou, Z. Hua, J. Shi, Q. He, L. Guo, M. Ruan, Chem. Eur. J. 15 (2009) 12949;
(e) Y. Zhu, Z. Hua, Y. Song, W. Wu, X. Zhou, J. Zhou, J. Shi, J. Catal. 299 (2013) 20;
(f) Y. Zhu, Z. Hua, J. Zhou, L. Wang, J. Zhao, Y. Gong, W. Wu, M. Ruan, J. Shi, Chem. Eur. J. 17 (2011) 14618.
[14] (a) H. Vezin, A. Moissette, C. Bremard, Angew. Chem. Int. Ed. 115 (2003) 5745;
(b) R.V. Chatti, N. Dubey, M.V. Joshi, N.K. Labhsetwar, P.N. Joshi, S.S. Rayalu, Int. J. Hydrogen Energy 35 (2010) 1911.
[15] (a) K. Moller, B. Yilmaz, U. Muller, T. Bein, Chem. Mater. 23 (2011) 4301;
(b) F. Xiao, L. Wang, C. Yin, K. Lin, J. Yan Di, R. Li, D. Xu, R. Su, T. Schlgl, T. Yokoi, Tatsumi, Angew. Chem. Int. Ed. 118 (2006) 3162.
[16] R. Barthos, F. Lonyi, Gy. Onyestyak, J. Valyon, Solid State Ionics 141–142 (2001) 253.
[17] (a) K. Maeda, M. Higashi, D. Lu, R. Abe, K. Domen, J. Am. Chem. Soc. 132 (2010) 5858;
(b) M. Higashi, K. Domen, R. Abe, J. Am. Chem. Soc. 134 (2012) 6968;
(c) S. Yang, L. Ma, Z. Fang, R. Vajtai, X. Wang, P.M. Ajayan, Adv. Mater. (2013), http://dx.doi.org/10.1002/adma.201204453.
[18] K. Zhang, H.R. Chen, X.X. Zhou, Y. Gong, G.B. Zhang, X. Wang, Y. Chen, J.L. Shi, J. Mater. Chem. A 2 (2014) 1515.
[19] J.L. Shi, Chem. Rev. 113 (2013) 2139.